https://doi.org/10.1016/j.intermet.2018.01.023

Atomistic deformation mechanisms of amorphous/polycrystalline metallic nanolaminates

L. Zhao, K.C. Chan*, S.H. Chen

Advanced Manufacturing Technology Research Centre, Department of Industrial and Systems Engineering, The Hong Kong Polytechnic University, Hung Hom, Kowloon, Hong Kong

Submitted to

Intermetallics

As a full paper

∗ Corresponding author.

E-mail address: kc.chan@polyu.edu.hk (K.C. Chan).

Abstract

A series of multilayer amorphous $Cu_{50}Zr_{50}$/Cu nanolaminates with consideration of grain boundary characteristics in the Cu layers were constructed and compressed to investigate the atomistic mechanisms of yielding and plastic deformation behavior using large-scale atomistic simulations. The results revealed that yielding occurs initially in the Cu layers through lattice dislocations, while plastic deformation in the amorphous layers is induced by the transfer of dislocation plasticity from the Cu layers, mainly at the intersections of the crystalline-amorphous interfaces and grain boundaries. Similar to the roles of defects-like secondary phases, the Cu layers serve as sites for heterogeneous nucleation of embryonic shear bands, as well as barriers to their propagation into mature ones. The coupled interplay between the crystal plasticity and the glassy plasticity in the nanolaminates promotes a more homogeneous redistribution of plastic deformation, providing a kind of hardening mechanism. In addition, our simulations also demonstrate a transition of the deformation mode from localized to homogeneous-like deformation by tailoring the relative volume fraction of the Cu layers. The findings provide more detailed atomistic information for understanding the underlying deformation mechanisms that are difficult to obtain by post-mortem observations and are useful for optimizing the structure of amorphous/crystalline metallic nanolaminates.

Keywords: Metallic glasses; Amorphous/crystalline metallic nanolaminate; Molecular dynamics simulations; Mechanical deformation

1. Introduction

Metallic glasses (MGs) have many attractive mechanical and physical properties that include high strength and elasticity, high hardness combined with excellent corrosion resistance [1-3]. However, one major impediment in utilizing MGs is the lack of ductility in comparison with their crystalline counterparts [4-6]. In the absence of microstructures that induces strain hardening and internal barriers such as grains boundaries as observed in crystalline metals, plastic deformation of most MGs at room temperature is usually localized into individual shear bands (SBs), which propagate unhindered to the extent that negligible macroscopic plasticity is experienced before catastrophic failure [7-9]. One promising route to alleviate this problem is to incorporate alternating crystalline metal layers to form periodically modulated multilayer nanostructures, i.e., amorphous/crystalline (a/c) nanolaminates, where the "defect-like" crystalline layers promote strain delocalization [10, 11]. Recently, numerous a/c nanolaminates, such as CuZr/Cu [12-15], PdSi/Cu [16, 17], CuNb/Cu [18], have been experimentally synthesized and their mechanical properties have been extensively probed [12-14, 16-20]. Through micropillar compression on CuZr/Cu nanolaminates with varied Cu layer thickness (10~100 nm), Guo et al. [20] found that the 100 nm-CuZr/50 nm-Cu nanolaminate exhibited a flow stress comparable to the strength of monolithic MGs while achieving a fracture strain exceeding 40%. Zhang et al. [13] compressed a series of micropillars laminated with equal layer thickness (5~50 nm) and revealed a transition of the deformation mode from pronounced shear banding to homogeneous-like co-deformation with increasing layer thickness. Knorr et al. [16] also revealed that the deformation morphologies of the multilayered architectures can be controlled by tuning the layer thickness as well as the relative volume fractions. These results have demonstrated great potential for tailoring a/c nanolaminates with a sought-after combination of improved plasticity and high strength. Although many previous reports pointed out that the plasticity improvement is greatly contributed to the cooperative deformation between amorphous layers and crystalline layers, the mechanistic insights were mainly based on speculation from post-mortem microstructure observations on post-deformed samples. The dilemma behind experimentation is that the details of the deformation process are tough to unravel since the plasticity carriers, such as the shear transformation zones (STZs), SBs and dislocations in the composites, are confined within narrow regions generally no more than 5~20 nm, and the transient

synergistic interactions among them could hardly be captured [11, 21]. All these make it difficult to fully understand the deformation behavior of the a/c nanolaminates.

On the other hand, atomistic modelling which allows one to directly investigate the detailed deformation behavior as a function of the tailored architectures from atomic-scale level and to effectively establish links between the underlying atomistic deformation mechanisms and corresponding mechanical properties, are a useful tool to supplement the experiments [22-25]. So far, certain researchers have applied large-scale molecular dynamics (MD) simulations to investigate the deformation behavior of a/c nanolaminates. In the tensile simulation of CuZr/Cu nanolaminate that contains a single crystal Cu layer, Wang et al. [11] found that crystalline-amorphous interfaces (CAIs) act as sources for nucleation of dislocations, and also demonstrate unique inelastic shear transfer characteristics that can induce STZs when impinged on by dislocations from the neighboring layer. This finding was also verified in simulation on compressing an a/c bilayer structure conducted by Arman et al. [26], who found that dislocations emitted near CAIs could directly induce a correlated SB pattern in amorphous layers across CAIs, thus resulting in a more stable shear banding process. The results of these pioneering simulation studies are instructive for understanding the deformation behavior of a/c nanolaminates. However, these adopted atomistic models were simplified either to be bilayer a/c structures or single crystal for the polycrystalline layers (without the presence of intrinsic GBs) [27, 28], so that the simulated deformation physics may not be fully bridged with actual experiments. Up to now, detailed atomistic investigation on the deformation behavior of multilayer amorphous/polycrystalline metal nanolaminates is yet to be undertaken.

In this study, a series of multilayer amorphous $Cu_{50}Zr_{50}$/polycrystalline Cu nanolaminates were constructed by tailoring the relative volume fractions of the Cu phases with consideration of GB characteristics to more closely resemble experimentally synthesized structures. Uniaxial compressive deformations were accomplished using MD simulations to investigate the deformation behavior, the underlying atomistic mechanisms of yielding and plasticity improvement, and the transition of the deformation mode from localized to homogeneous-like deformation in the multilayer nanostructures. Research emphasis was placed on the unique interplay between crystal plasticity and glassy plasticity in the two kinds of layers at the nanoscale. The findings provide a more detailed atomistic understanding of tailorable deformation behavior and mechanical properties

in the a/c nanolaminates.

2. Methods

MD simulations were performed utilizing LAMMPS [29]. Binary $Cu_{50}Zr_{50}$ MG and pure Cu, were chosen as the amorphous layers and crystalline layers, respectively. The interatomic interactions were described by the embedded-atom-method (EAM) potential developed by Sheng et al [30]. To construct a monolithic MG, a primitive $Cu_{50}Zr_{50}$ amorphous configuration, composed of 30000 atoms, was first prepared by quenching its melting liquid (2000 K) to the glassy state (100 K) at a cooling rate of 1×10^{10} K/s. The constant-pressure-temperature ensemble (*NPT*) and three-dimensional periodic boundary conditions (PBCs) and a time step of 2 fs were applied. The MG sample was then generated by replicating the as-cast configuration, followed by sub-T_g annealing at 600 K for 0.5 ns (T_g~715 K for $Cu_{50}Zr_{50}$ MG), and further brought back to 100 K. The final obtained monolithic MG, of dimensions ~$58.7\times5.3\times117.4$ nm^3, corresponds to a total atomic number of ~3 million. In constructing the a/c nanolaminates, the polycrystalline Cu layers, treated as a series of columnar grains with arbitrary crystallographic orientations, were generated by employing the Voronoi-tessellation method [31] using a single crystal Cu as the source of the material. Then, $Cu_{50}Zr_{50}$/Cu nanolaminates were constructed by incorporating these polycrystalline Cu layers into the monolithic MG. Atoms near the CAIs and GBs that overlapped with separation distances less than 2.0 Å were removed. The in-plane grain sizes of polycrystalline Cu approximate to the thickness of Cu layers to better represent the experimentally synthesized nanolaminates [32]. The nanograins are infinitely long columnar shapes along the Y-direction in view of the applied PBCs. The constructed nanolaminates were further annealed at 600 K for 0.5 ns by applying an external hydrostatic pressure of 1.5 GPa to generate more realistic interfaces and eliminate voids which may be generated during sample construction.

Uniaxial compressive simulations were conducted along the Z-direction via scaling the corresponding cell length at 100 K and a strain rate of 1×10^8 s^{-1}. Note that the effect of different deformation strain rates (1×10^8 s^{-1}, 2×10^8 s^{-1} and 5×10^8 s^{-1}) was examined and found that the strain rate mildly affects the peak strength and flow stress of the nanolaminates, but has no apparent influence on the deformation mechanism of the nanolaminates. A low temperature of 100 K was chosen to eliminate the effect of thermodynamic fluctuation and promote SBs formation under

loading, highlighting the responses upon mechanical activation in the superfast quenched MD samples [33, 34]. PBCs were imposed in three dimensions to mimic a bulk size and wipe off the free surface effects which may add complications on the deformation of the nanoscale samples [22, 26]. In addition, the normal stresses in the X-axis and Y-axis were relaxed to zero to allow lateral contraction during compression. The resultant stress was extracted from the normal tensor component of the virial stress along the loading direction [22].

To monitor the deformation process of the samples, the atomic-level deformation was monitored by local atomic shear strain, η^{Mises}, proposed by Shimizu [35]. Generally, regions mapped with relatively large η^{Mises} (i.e., η^{Mises} >0.2) indicate a collective inelastic shearing of local clusters of atoms in response to the applied strain and can be viewed as volumes of atoms involved in plastic deformation [22, 36]. To quantify the deformation degree, $\psi = N^{\eta>0.2}/N$, $\psi_g = N_g^{\eta>0.2}/N$ and $\psi_c = N_c^{\eta>0.2}/N$ was defined to quantify the fractions of atoms participating in the plastic deformation in the whole samples (ψ), in the amorphous layers (ψ_a) and Cu layers (ψ_c), where $N^{\eta>0.2}$, $N_g^{\eta>0.2}$, $N_c^{\eta>0.2}$ and N represents the number of atoms with $\eta^{Mises} > 0.2$ in the whole samples, the amorphous layers, Cu layers and the total atoms in the samples. To evaluate the deformation inhomogeneity of the nanolaminates, the strain localization parameter proposed by Cheng et al., [37] was introduced, $\delta = \sqrt{\frac{1}{N}\sum_{i=1}^{N}(\eta_i - \bar{\eta})^2}$, where $\bar{\eta}$ is the average atomic shear strain over all atoms in the samples. The δ value quantifies the overall deviation of the atomic strain distribution of the samples from homogeneous deformation in which case δ approaches 0. The local structural orders and dislocations in the Cu layers were distinguished by the common neighbor analysis method (CNA) [38, 39] and the so-called dislocation extraction algorithm (DXA) [40], respectively. The visualization was realized using OVITO [41].

3. Results and discussion

3.1. The structure of nanolaminates

In this study, we fabricated three a/c nanolaminates (hereafter labeled as sample “2L”, “4L”, “6L”), in which the corresponding numbers of polycrystalline Cu layers were embedded in the monolithic $Cu_{50}Zr_{50}$ MG, respectively. More specifically, the 2L, 4L and 6L nanolaminates have alternating

stacks of CuZr(47 nm)/Cu(10 nm), CuZr(18 nm)/C(10 nm) and CuZr(9 nm)/Cu(10 nm) bilayers, which corresponds to a volume fraction of 17.5%, 35.7% and 52.6% for the polycrystalline Cu phases, respectively. The final sub-T_g annealed a/c nanolaminates shown in Fig. 1 reveal that almost all the nanograins (average grain size ~10 nm) in the polycrystalline Cu layers are in perfect face-centered cubic (FCC) structure. Only trace amounts of atoms are in stacking faults which are preferably located in the CAIs and GBs due to mismatched crystal lattices, and few have dislocations or twin defects within the nanograins generated during the preparation. The defects-free samples can serve as ideal models to investigate the interactive co-deformation between the amorphous layers and crystalline layers, and structural evaluation in the a/c multilayer nanostructures from the atomistic viewpoint.

Through uniaxial compression of these tailored samples, we examined the atomistic mechanisms governing the yielding and tunable plasticity in the nanolaminates. Recent experiments on nano/mircopillar compression reported that similar a/c nanolaminates could achieve failure strains higher than 40 % [20, 42], while in our MD simulations, no obvious fracture could be observed on the nanolaminates under even more severe deformation. Thus, similar to the previous work [36, 43], the plasticity described in this study was evaluated by the magnitude of the stress drop after global yielding in the stress-strain (SS) curves, and the strain localization parameter (see Methods).

3.2. The SS response of nanolaminates

Fig. 2(a) illustrates the compressive SS curves for the series of nanolaminates along with the monolithic MG, for comparison. To quantify the process of plasticity accumulation, the evolution of the deformation degree in all the samples as a function of the applied strain is also depicted in Fig. 2(b). One can clearly find disparities in the deformation behavior by introducing heterogeneous Cu layers in the monolithic MG. In the elastic response regime, ψ remain approximately zero, which indicates negligible inelastic deformation at low applied strains. While, the initial linear SS relationships reveal that the elastic modules of the nanolaminates (E=74 GPa, 82 GPa and 88 GPa for sample 2L, 4L and 6L, respectively) are higher than that for the monolithic MG (E=69 GPa) and augment monotonously with the numbers of Cu layers, i.e., their relative volume frictions (E=98 GPa for nanocrystalline Cu [21]). This tendency is in good agreement with the rule-of-mixtures prediction. In addition, the nanolaminates tend to yield earlier as revealed in Fig. 2(a), consistent with the previous experimental reports [19, 44]. Correspondingly, lower critical strains, at which ψ

begin to increase, is probed for the nanolaminates in Fig. 2(b). In general, increasing the volume fraction of the Cu layers, like the addition of more structural defects in the nanolaminates, thus leading to easier activation of inelastic deformation, which should naturally result in earlier global yielding [22].

More noticeable differences in the plastic flow behavior can be observed for the nanolaminates in contrast to the monolithic MG. In all, the nanolaminates show a decreasing tendency both in the yielding stress (σ_y) and the peak strength (σ_p) with increasing numbers of Cu layers (0L→6L). However, the SS curves clearly demonstrate a more moderate stress drop ($\Delta=\sigma_p-\sigma_f$) after the peak strength and higher average flow stress (σ_f) at the post-yielding stage ($\varepsilon > 7.5\%$), a manifestation of improved plasticity by introducing heterogeneous Cu layers. Meanwhile, as shown in Fig. 2(b), after yielding ψ increases in a manner more proportional to the applied strain and shows larger values, which indicates that more atoms are involved in plastic deformation with increasing the numbers of Cu layers. The SS curves clearly reveal that the mechanical properties of the nanolaminates can be controlled by tuning the relative volume fraction of the Cu layers at the expense of some strength. Using the 4L nanolaminate as an example, although its peak strength is 16% lower than that of the monolithic MG (3.1 GPa VS. 3.6 GPa), the subsequent stress drop decreases by one half (1.6 GPa VS. 0.8 GPa) and the ψ at strain 17% increases by 88 % (0.25 VS. 0.47). In the SS curves, one also can observe more apparent serrated flow at the post-yielding stage for the nanolaminates, in contrast to the smoother, lower and even successive descending tendency displayed in the monolithic MG. The deformation mechanisms of monolithic MGs have been extensively investigated so far, with a consensus that the sharp drop in stress in monolithic MGs is correlated with the rapid spontaneous localization of severe shear deformation into single narrow SB, and has been regarded as a characteristic of poor plasticity [45, 46]. The decline tendency in the flow stress is attributed to the nature of shear-induced softening, dilatation as well as rapid heating within the operating SBs due to the lack of hardening mechanisms in its intrinsic structureless configuration [47-49]. While, the apparent serrated flow in the nanolaminates, as observed in this study, clearly indicate the existence of simultaneous competition of strain-induced softening and hardening in the amorphous layers and crystalline layers. The SS results strongly support a more non-localized deformation mode in the nanolaminates and reveal that a sought-after combination of high strength and promoted plasticity can be tailored by introducing a certain amount of Cu layers.

3.3. Mechanism of yielding

To further uncover the underlying atomistic mechanisms governing the tunable deformation behaviors in the nanolaminates, as an illustrative case, the 4L sample under different applied strains are demonstrated in Fig. 3 via η^{Mises} together with CNA. We first examine the physical origin of plastic yielding in the two distinct types of layers. The atomic-level deformation and structural configuration in Fig. 3 reveals that plastic deformation occurs initially in the crystalline Cu layers through the deposition of lattice dislocations (mainly Shockley partials). Notably, these dislocations tend to be activated easily in Cu grains which have more favorable lattice orientations for shearing along the maximum shear stress. And their nucleation sites are preferably located in the vicinity of CAIs and GBs since lower activation energy is required to activate dislocations in these defects-like regions. In this process, due to the lack of strain hardening in the initial defect-free Cu grains, these dislocation events are registered as a series of local stress drops in the SS curves before the formation of embryonic SBs in amorphous layers. It is also interesting to observe that most of the lattice dislocations are impeded upon impinging on the CAIs, as shown in Fig. 3(a) at ε =4.2%. Correspondingly, in the amorphous layers, a series of atomic rearrangements via localized STZs plasticity are activated to accommodate the local shear deformation carried by the dislocations. With increasing loading, dislocations are continuously activated in the adjacent parallel or even intersecting slip planes, and more grains are simultaneously involved in plastic deformation (see Video S1 in Supplementary Materials). During this stage, plasticity mainly via nucleation and slips of dislocations is constrained within the polycrystalline Cu layers. When the applied strain is sufficiently large, e.g., ε =7.0%, the dislocations successfully trigger several embryonic SBs, such as those marked by the white arrows in Fig. 3(a), leading to the transfer of plastic strain across the CAIs into the amorphous layers. Note that most of the embryonic SBs tend to be induced by the dislocations in a correlated fashion at the intersections of the CAIs and GBs, except the one denoted as “4”, which is generated near the simple CAIs (interfaces away from the GBs). In general, the unique GBs-CAIs triple junctions promote the formation of stress concentrations and strain mismatches, thus leading to the biasing of SBs activation sites to these regions. Our simulations reveal that the intersections of the CAIs and GBs, rather than any sites in the CAIs, tend to be the dominating sources of plastic shear transfer between the two kinds of layers in a/c nanolaminates.

It should be emphasized that our results on the yielding behavior of a/c nanolaminates is quite different from previous MD studies using single crystal Cu/CuZr amorphous structures [27, 50, 51], in which a tendency of initial yielding in the amorphous layers was observed. Note that their models were simplified without considering the presence of GBs, which is in fact a critical characteristic in the nanocrystalline Cu phases and can greatly affect the deformation behavior [21, 52]. It is well documented in experiments that the yielding strain and stress as well as the maximum strength of nanocrystalline Cu are much lower than those of perfect single crystal Cu and CuZr MGs [11]. To validate this standpoint in MD analysis, we performed uniaxial compressive simulations on a pure nanocrystalline Cu (NC) with an average grain size of ~10 nm and a single crystal Cu (SC) with its [111] plane along the loading direction. The obtained SS curves shown in Fig. 4 clearly reveal the same relative relationship of strength between the nanocrystalline Cu and $Cu_{50}Zr_{50}$ MG, but display the largest yielding stress for the single crystal Cu. Based on this result, it is conceivable that under the same applied stress, the nanocrystalline Cu should yield first, then follows the $Cu_{50}Zr_{50}$ MG and the single crystal Cu. The simplification of the Cu layers into single crystal in the nanolaminates unduly strengthens the Cu layers, thus resulting in different deformation behaviors of the nanolaminates.

3.4. Coupling between crystal plasticity and glassy plasticity

We further focus on the mechanism of plastic improvement in the 4L nanolaminate with an emphasis on the interplay between crystal plasticity and glassy plasticity in the two kinds of layers. As the embryonic SBs are triggered, they tend to propagate along favorable paths under loading. We can observe that the initial propagation directions of the embryonic SBs are in compliance with the dislocation slip planes, i.e., approximate 45° relative to the loading direction. When the SBs penetrate the corresponding amorphous layers and extend into the adjacent Cu layers across the CAIs, they encounter the Cu nanograins before propagating very far. The Cu nanograins appear to provide effective barriers to the SBs propagation and slow down the SBs dynamics [19], playing a role similar to that of secondary phases with dislocations in the crystalline metals. As shown in Fig. 3(a) at ε =10.0%, one can clearly observe the suppression, deflection and bifurcation of the local operating embryonic SBs in the amorphous layers. For example, SBs marked as “6” and “8” cease propagation by decomposing their shear fronts into several dislocations, resulting in intersecting dislocations slip in the nanograins; SBs marked as “4” and “5” deviate from the original shear

planes by branching near the Cu layers; while SBs marked as “1” and “3” tend to deflect the deformation along the GBs or CAIs upon impinging on the grain boundaries. In all, most of the embryonic SBs are arrested by the Cu layers with few directly penetrating the Cu nanograins. The interactions of propagating SBs with Cu layers suppress the formation of mature SBs as well as the onset of shear instability. In turn, more secondary SBs and dislocations are activated simultaneously nearby the CAIs to accommodate the local plastic deformation associated with the blocked SBs. This kind of coupling activation of SBs and dislocations between the amorphous layers and Cu layers tend to be more pronounced under extensive deformation, as evidenced by the abundant viable interlacing shear and slip bands at ε =17.0%. The cooperative deformation promotes the redistribution of plasticity between the two phases and brings more materials into the process of plastic deformation. Therefore, more energy can be dissipated and the deformation can be more homogeneous. Moreover, the unique cooperative deformation provides a kind of hardening mechanism in the nanolaminates, partially alleviating strain-induced softening associated with shear localization in the glassy layers [22], thus resulting in higher flow stress as observed in Fig. 2(a).

In this study, via the CNA method, the locations of the CAIs as well as the local structural evolution in the 4L nanolaminate during plastic deformation can be effectively detected. In line with previous experimental micro-pillar compressions [16, 44], thinning in layer thickness (distance between two adjacent CAIs) can be clearly observed for both types of layers as revealed in Fig. 3(b). While the co-deformation between the two layers is quite nonuniform due to the intrinsic characteristic of localized interactions between dislocations and SBs. As a result, the original straight CAIs become wavy in shape under large applied strain, as shown at ε=17.0% in Fig. 3(b). Meanwhile, dislocation-mediated grain rotations (such as those labelled as “A” and “B”) are also observed in the grains undergoing large local shear deformation. These deformation features combined with the structural defects align with post-mortem TEM observations on CuZr/Cu [13, 19] and PdSi/Cu [16] nanolaminates. Interestingly, the rotating grains tend to be the ones which emit dislocations earlier in the initial yielding stage of the nanolaminates. Under continuous compressive deformation, their lattice orientations related to the CAIs decrease gradually with the deformation process.

We also present a quantitative interpretation of the relative strain evolution in the 4L nanolaminate by providing the evolution of the deformation degrees in the amorphous layers (ψ_a) and the crystalline Cu layers (ψ_c), as demonstrated in Fig. 5. In general, ψ_a and ψ_c augment monotonously

with the deformation after yielding, while a crossover can be observed at the strain ~7.5% (ε_c), which is close to the end of the stress drop after the peak stress. Accordingly, the deformation process of the nanolaminate can be divided into 3 stages, consistent with the experiments on MG matrix composites [36, 53, 54]. In the 1st stage ($\varepsilon<\varepsilon_y$), ψ_a and ψ_c remain approximately zero, reflecting uniform elastic deformation both in the amorphous layers and crystalline Cu layers. In the 2nd stage ($\varepsilon_y<\varepsilon<\varepsilon_c$), ψ_c increases rapidly at first due to the initial yielding in the Cu layers. Although many STZs and embryonic SBs are subsequently triggered in the amorphous layers by the dislocation slips near the intersection regions between the CAIs and GBs, ψ_c still show a higher value than ψ_a at any given strain. This indicates that crystal plasticity dominates the plasticity deformation in the nanolaminate in this range. In the 3rd stage ($\varepsilon>\varepsilon_c$), upon exceeding the crossover, ψ_a become larger than ψ_c, inversely. The suppression, deflection and bifurcation of the operating SBs by the Cu layers results in multiple secondary SBs and dislocations. Hence, a more collective homogeneous distribution of plasticity deformation is involved in the amorphous layers, and glassy plasticity begins to play the dominating role in the plasticity of the nanolaminate. The relative evolution of ψ_a and ψ_c clearly reveals that glassy plasticity in the amorphous layers is closely linked with crystal plasticity in Cu layers. More specifically, the Cu layers in the nanolaminate act as heterogeneous nucleation sites of multiple STZs and SBs as well as barriers to their propagation, thus resulting in non-localized plastic deformation.

3.5. Transition from localized to homogeneous-like deformation

From above analysis of the 4L nanolaminate, one can recognize the mechanisms of yielding and plastic deformation in the periodically modulated a/c nanostructures. While, the failure modes of the nanolaminates vary with different volume fractions of Cu layers [13, 16, 20]. It was previously reported that SB, associated with relative sliding of two or several parts of the material, is the primary cause for plastic deformation and the failure of monolithic glasses and their composites [22, 55]. To reveal the influence of the relative volume fractions of the Cu layers on the morphology of the SBs, Fig. 6 demonstrates the configurations of the monolithic MG, 2L, 4L and 6L nanolaminates at ε=17.0%. one can clearly see that the morphology of the SBs in the nanolaminates can be effectively controlled by tuning the volume fraction of the crystalline Cu phase. For the monolithic MG shown in Fig. 6(a), three parallel mature SBs are generated by stochastic nucleation, coalescence and growth of STZs in the sample [46]. Due to the absence of hardening mechanisms

in the disordered structure, the SBs penetrate the whole sample soon after the formation of embryonic SBs without any impediment. Since plastic deformation is mainly concentrated in the ~10 nm-thick SBs, the strain localization combined with incidental shear instability leads to catastrophic failure for the monolithic MG with limited plasticity [4, 46]. Embedding Cu layers in the brittle monolithic MG can promote the formation of multiple STZs and SBs, leading to a more evenly distributed plastic deformation. As shown in Fig. 6(b), for the 2L sample with a low volume fraction of the Cu phases (17.5%), several well-defined interlayer SBs are generated due to the insufficient suspension effect from the Cu layers. While, an intersecting pattern of the SBs is observed, which is necessary for achieving large plasticity in MGs and their composites [4, 22]. With increasing volume fraction of the Cu phases, the possibility associated with the development of mature SBs that penetrate multiple layers is suppressed, since more energy is dissipated in triggering secondary SBs and dislocations. Thus, at a Cu volume fraction of 35.7% (4L), few SBs can effectively penetrate the underlying Cu layers by more than 2 layers. More remarkably, with the highest volume fraction of the Cu layers reaching 52.6% (6L) in this study, the initiated local SBs are fully confined within separated small glassy sub-domains. As a result, a high density of local networks of tiny SBs and dislocations are observed. It can be seen that a transition of deformation modes from pronounced individual shear banding to homogeneous-like co-deformation can be achieved by increasing the volume fractions of the Cu layers in the nanolaminates.

Fig. 7 displays the strain localization parameter (δ) of the series of nanolaminates at an applied strain of 17% to evaluate the influence of relative volume fractions of Cu phases on the overall deformation inhomogeneity. In general, a larger δ implies a higher propensity for localized deformation, leading to poorer plasticity. It is clearly revealed that δ decreases in the order of the monolithic MG, 2L, 4L, 6L, i.e., the plastic deformation tends to be more homogeneous with increasing volume frictions of the Cu phases. The introduced polycrystalline Cu layers serve as sites for heterogeneous nucleation of glassy plasticity, as well as barriers to the propagation of embryonic SBs into mature ones. Therefore, more plastic deformation can be effectively promoted by redistributing the plasticity into more materials, thereby resulting in a lower δ. The evolution of δ provides clear evidence for the effect of the crystalline Cu layers on shear delocalization in the nanolaminates. From these simulation results, one can recognize the significance of optimizing the volume fraction of the crystalline layers in enhancing the global plasticity and strength of a/c

nanolaminates.

4. Conclusions

In this work, the compressive deformation behaviors of three a/c multilayer nanolaminates having different volume fraction of Cu layers were investigated by MD simulation. Significant insights were gained into understanding the underlying atomistic mechanisms of yielding and tunable plasticity in the nanolaminates. It is found that the mechanical properties of the nanolaminates can be effectively tuned by introducing heterogeneous “defect-like” Cu layers, but at the expense of strength. In general, yielding of the nanolaminates occurs initially in the Cu layers through the emitting of lattice dislocations, which further trigger plastic deformation in the amorphous layers via formation of multiply embryonic SBs through the transfer of crystal plasticity at locations mainly near the CAIs-GBs triple junctions. The Cu layers provide effective sources for SBs formation as well as barriers for their propagation, leading to the suppression, deflection and bifurcation of the local operating SBs. The origin of the improved plasticity is contributed by the coupled interplay between the crystal plasticity and the glassy plasticity at the nanoscale, which promotes the redistribution of plasticity, providing a kind of hardening mechanism in the nanolaminates. Our results demonstrate that tailoring the relative volume fraction of the Cu layers could be an effective approach for tuning the plasticity in a/c nanocomposites.

Acknowledgements

This research was fully funded by the Research Committee of the Hong Kong Polytechnic University under research student project account code RTLR.

References

[1] Schuh CA, Hufnagel TC, Ramamurty U. Mechanical behavior of amorphous alloys. Acta Mater. 2007;55:4067-109.

[2] Inoue A, Takeuchi A. Recent development and application products of bulk glassy alloys. Acta Mater. 2011;59:2243-67.

[3] Wang WH, Dong C, Shek CH. Bulk metallic glasses. Mater Sci Eng, R. 2004;44:45-89.

[4] Greer AL, Cheng YQ, Ma E. Shear bands in metallic glasses. Mater Sci Eng, R. 2013;74:71-132.

[5] Lewandowski J, Wang W, Greer A. Intrinsic plasticity or brittleness of metallic glasses. Philos Mag Lett. 2005;85:77-87.

[6] Axinte E. Metallic glasses from " alchemy" to pure science: Present and future of design, processing and applications of glassy metals. Mater Des. 2012;35:518-56.

[7] Steif PS, Spaepen F, Hutchinson JW. Strain localization in amorphous metals. Acta Metall. 1982;30:447-55.

[8] Bei H, Xie S, George EP. Softening caused by profuse shear banding in a bulk metallic glass. Phys Rev Lett. 2006;96:105503.

[9] Chen SH, Chan KC, Xia L. Deformation behavior of a Zr-based bulk metallic glass under a complex stress state. Intermetallics. 2013;43:38-44.

[10] Kim JY, Jang D, Greer JR. Nanolaminates Utilizing Size‐Dependent Homogeneous Plasticity of Metallic Glasses. Adv Funct Mater. 2011;21:4550-4.

[11] Wang Y, Li J, Hamza AV, Barbee TW. Ductile crystalline–amorphous nanolaminates. Prov Natl Acad Sci. 2007;104:11155-60.

[12] Zhang JY, Liu G, Sun J. Self-toughening crystalline Cu/amorphous Cu-Zr nanolaminates: Deformation-induced devitrification. Acta Mater. 2014;66:22-31.

[13] Zhang J, Liu G, Lei S, Niu J, Sun J. Transition from homogeneous-like to shear-band deformation in nanolayered crystalline Cu/amorphous Cu-Zr micropillars: Intrinsic vs. extrinsic size effect. Acta Mater. 2012;60:7183-96.

[14] Guo W, Yao J, Jägle EA, Choi PP, Herbig M, Schneider JM, et al. Deformation induced alloying in crystalline-metallic glass nano-composites. Mater Sci Eng, A. 2015;628:269-80.

[15] Cui Y, Abad OT, Wang F, Huang P, Lu T-J, Xu K-W, et al. Plastic deformation modes of CuZr/Cu multilayers. Sci Rep. 2016;6:23306.

[16] Knorr I, Cordero N, Lilleodden ET, Volkert CA. Mechanical behavior of nanoscale Cu/PdSi multilayers. Acta Mater. 2013;61:4984-95.

[17] Donohue A, Spaepen F, Hoagland R, Misra A. Suppression of the shear band instability during plastic flow of nanometer-scale confined metallic glasses. Appl Phys Lett. 2007;91:241905.

[18] Fan Z, Xue S, Wang J, Yu K, Wang H, Zhang X. Unusual size dependent strengthening mechanisms of Cu/amorphous CuNb multilayers. Acta Mater. 2016;120:327-36.

[19] Guo W, Gan B, Molina-Aldareguia JM, Poplawsky JD, Raabe D. Structure and dynamics of

shear bands in amorphous-crystalline nanolaminates. Scripta Mater. 2016;110:28-32.

[20] Guo W, Jägle E, Yao J, Maier V, Korte-Kerzel S, Schneider JM, et al. Intrinsic and extrinsic size effects in the deformation of amorphous CuZr/nanocrystalline Cu nanolaminates. Acta Mater. 2014;80:94-106.

[21] Cheng B, Trelewicz JR. Mechanistic coupling of dislocation and shear transformation zone plasticity in crystalline-amorphous nanolaminates. Acta Mater. 2016;117:293-305.

[22] Zhou H, Qu S, Yang W. An atomistic investigation of structural evolution in metallic glass matrix composites. Int J Plast. 2013;44:147-60.

[23] Gupta P, Pal S, Yedla N. Molecular dynamics based cohesive zone modeling of Al (metal)–Cu50Zr50 (metallic glass) interfacial mechanical behavior and investigation of dissipative mechanisms. Materials & Design. 2016;105:41-50.

[24] Adibi S, Branicio PS, Ballarini R. Compromising high strength and ductility in nanoglass–metallic glass nanolaminates. RSC Advances. 2016;6:13548-53.

[25] Sha ZD, Branicio PS, Lee HP, Tay TE. Strong and ductile nanolaminate composites combining metallic glasses and nanoglasses. Int J Plast. 2017;90:231-41.

[26] Arman B, Brandl C, Luo S, Germann T, Misra A, Çağin T. Plasticity in Cu (111)/Cu46Zr54 glass nanolaminates under uniaxial compression. J Appl Phys. 2011;110:043539.

[27] Song HY, Xu JJ, Zhang YG, Li S, Wang DH, Li YL. Molecular dynamics study of deformation behavior of crystalline Cu/amorphous Cu50Zr50 nanolaminates. Materials & Design. 2017;127:173-82.

[28] Gupta P, Pal S, Yedla N. Molecular dynamics based cohesive zone modeling of Al (metal)-Cu50Zr50 (metallic glass) interfacial mechanical behavior and investigation of dissipative mechanisms. Materials & Design. 2016;105:41-50.

[29] Plimpton S. Fast parallel algorithms for short-range molecular dynamics. J Comput Phys. 1995;117:1-19.

[30] Cheng Y, Ma E, Sheng H. Atomic level structure in multicomponent bulk metallic glass. Phys Rev Lett. 2009;102:245501.

[31] Li J. AtomEye: an efficient atomistic configuration viewer. Modell Simul Mater Sci Eng. 2003;11:173.

[32] Guo W, Jägle EA, Choi P-P, Yao J, Kostka A, Schneider JM, et al. Shear-induced mixing

governs codeformation of crystalline-amorphous nanolaminates. Phys Rev Lett. 2014;113:035501.

[33] Cheng YQ, Cao AJ, Sheng HW, Ma E. Local order influences initiation of plastic flow in metallic glass: Effects of alloy composition and sample cooling history. Acta Mater. 2008;56:5263-75.

[34] Zhong C, Zhang H, Cao Q, Wang X, Zhang D, Ramamurty U, et al. Deformation behavior of metallic glasses with shear band like atomic structure: a molecular dynamics study. Sci Rep. 2016;6.

[35] Shimizu F, Ogata S, Li J. Theory of shear banding in metallic glasses and molecular dynamics calculations. Mater Trans. 2007;48:2923-7.

[36] Jian W, Wang L, Li B, Yao X, Luo S. Improved ductility of Cu64Zr36 metallic glass/Cu nanocomposites via phase and grain boundaries. Nanotechnology. 2016;27:175701.

[37] Cheng Y, Cao A, Ma E. Correlation between the elastic modulus and the intrinsic plastic behavior of metallic glasses: The roles of atomic configuration and alloy composition. Acta Mater. 2009;57:3253-67.

[38] Faken D, Jónsson H. Systematic analysis of local atomic structure combined with 3D computer graphics. Comput Mater Sci. 1994;2:279-86.

[39] Tsuzuki H, Branicio PS, Rino JP. Structural characterization of deformed crystals by analysis of common atomic neighborhood. Computer Physics Communications. 2007;177:518-23.

[40] Stukowski A, Bulatov VV, Arsenlis A. Automated identification and indexing of dislocations in crystal interfaces. Modell Simul Mater Sci Eng. 2012;20.

[41] Stukowski A. Visualization and analysis of atomistic simulation data with OVITO-the Open Visualization Tool. Modell Simul Mater Sci Eng. 2009;18:015012.

[42] Zhang J, Wang Y, Liu G, Sun J. Plastic deformation characteristics of Cu/X (X Cu Zr, Zr) nanolayered materials. Appl Surf Sci. 2014;321:19-23.

[43] Sha ZD, He LC, Pei QX, Liu ZS, Zhang YW, Wang TJ. The mechanical properties of a nanoglass/metallic glass/nanoglass sandwich structure. Scripta Materialia. 2014;83:37-40.

[44] Liu M, Du X, Lin I, Pei H, Huang J. Superplastic-like deformation in metallic amorphous/crystalline nanolayered micropillars. Intermetallics. 2012;30:30-4.

[45] Zhong C, Zhang H, Cao QP, Wang XD, Zhang DX, Jiang JZ. The size-dependent non-localized deformation in a metallic alloy. Scripta Materialia. 2015;101:48-51.

[46] Cao AJ, Cheng YQ, Ma E. Structural processes that initiate shear localization in metallic glass. Acta Mater. 2009;57:5146-55.

[47] Wang YJ, Jiang MQ, Tian ZL, Dai LH. Direct atomic-scale evidence for shear-dilatation correlation in metallic glasses. Scripta Mater. 2016;112:37-41.

[48] Peng HL, Li MZ, Wang WH. Stress-versus temperature-induced structural evolution in metallic glasses. Appl Phys Lett. 2013;102.

[49] Shi Y, Falk ML. Stress-induced structural transformation and shear banding during simulated nanoindentation of a metallic glass. Acta Mater. 2007;55:4317-24.

[50] Cui Y, Shibutani Y, Li S, Huang P, Wang F. Plastic deformation behaviors of amorphous-Cu50Zr50/crystalline-Cu nanolaminated structures by molecular dynamics simulations. J Alloys Compd. 2017;693:285-90.

[51] Luan YW, Li CH, Zhang D, Li J, Han XJ, Li JG. Plastic deformation mechanisms and size effect of Cu50Zr50/Cu amorphous/crystalline nanolaminate: A molecular dynamics study. Comput Mater Sci. 2017;129:137-46.

[52] Schiøtz J, Di Tolla FD, Jacobsen KW. Softening of nanocrystalline metals at very small grain sizes. Nature. 1998;391:561-3.

[53] Wu FF, Chan KC, Jiang SS, Chen SH, Wang G. Bulk metallic glass composite with good tensile ductility, high strength and large elastic strain limit. Sci Rep. 2014;4.

[54] Wu FF, Wei J, Chan K, Chen S, Zhao R, Zhang G, et al. Revealing homogeneous plastic deformation in dendrite-reinforced Ti-based metallic glass composites under tension. Sci Rep. 2017;7.

[55] Şopu D, Stoica M, Eckert J. Deformation behavior of metallic glass composites reinforced with shape memory nanowires studied via molecular dynamics simulations. Appl. 2015;106.

Figures

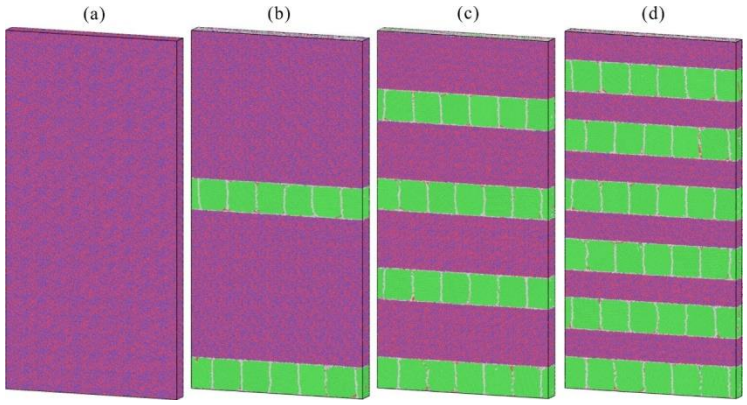

Figure 1. The atomic configurations of sub-T_g annealed a/c nanolaminates consisting of different layers of polycrystalline Cu phases. (a) the monolithic MG, (b) 2L-CuZr(47 nm)/Cu(10 nm), (c) 4L-CuZr(18 nm)/Cu(10 nm) and (d) 6L-CuZr(9 nm)/Cu(10 nm). Atoms in the Cu layers are labeled by their local atomic coordination, i.e., green for atoms with face-centered cubic coordination, red for atoms with hexagonal close-packed coordination (usually atoms in stacking faults) and grey for atoms around the CAIs and GBs. (For interpretation of the references to color in this figure legend, the reader is referred to the web version of this article.)

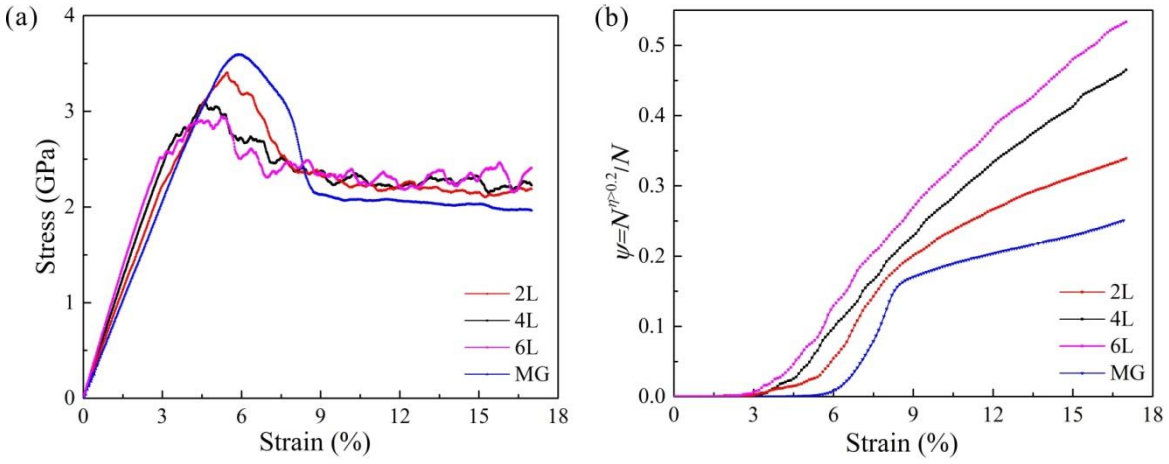

Figure 2. (a) Uniaxial compressive SS curves for the a/c nanolaminates and the monolithic MG at the strain rate of 1×10^8 s^{-1}; (b) The evolution of ψ against the applied strain. ψ is defined as the relative number of atoms with η larger than 0.2 with respect to the total atomic numbers in the samples.

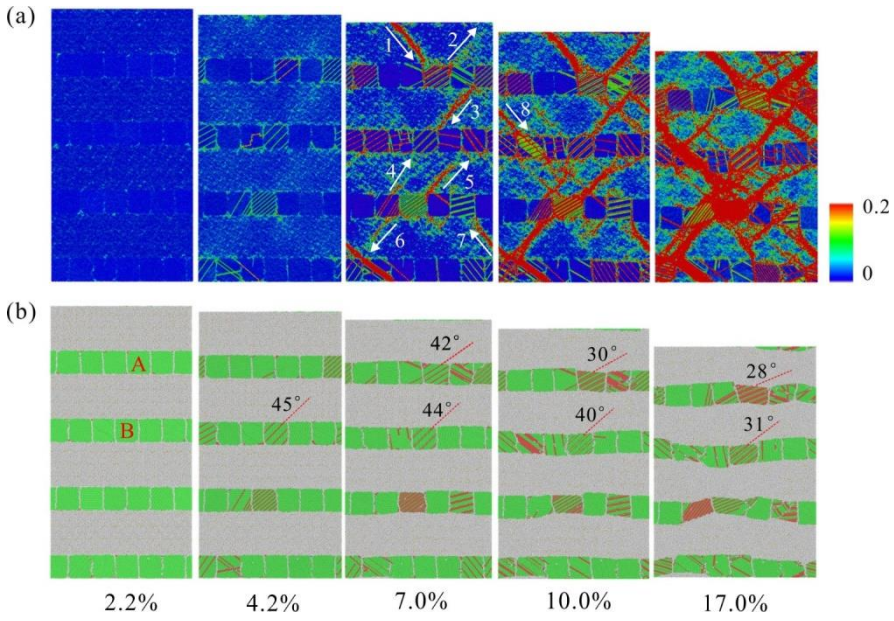

Figure 3. (a) Snapshots of atomic configurations under different applied strain via η^{Mises} demonstrating the deformation process for the 4L nanolaminate. (b) The structural evolution in the Cu layers and the location of the CAIs monitored by CNA. Note that the white arrows denote the nucleation sites as well as the propagation directions of the embryonic SBs. (For interpretation of the references to color in this figure legend, the reader is referred to the web version of this article.)

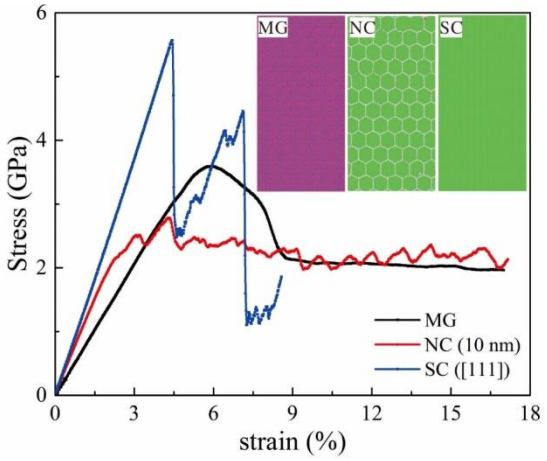

Figure 4. Uniaxial compressive SS curves for the monolithic MG, the pure nanocrystalline Cu and the single crystal Cu at the strain rate of 1×10^{8} s^{-1}. The insets demonstrate the snapshot of their atomic configurations.

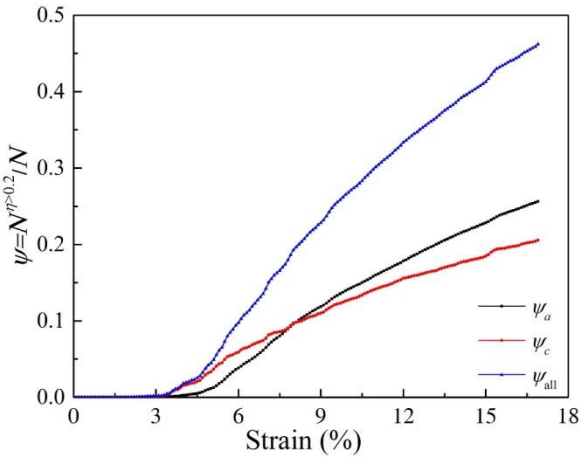

Figure 5. Comparison of ψ in the amorphous layers and Cu layers for the 4L nanolaminate. ψ is defined as the relative number of atoms with η larger than 0.2 with respect to the atomic number in the corresponding kind of layers.

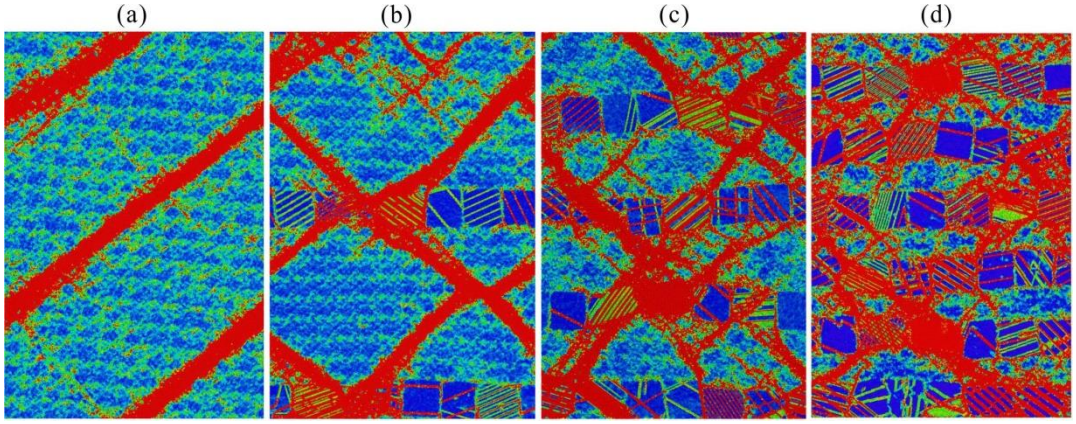

Figure 6. The final deformation configurations of (a) the monolithic MG, (b) 2L, (c) 4L and (d) 6L nanolaminates at an applied strain of 17%, revealing the morphology of the SBs. The atoms are colored by η^{Mises}. (For interpretation of the references to colour in this figure legend, the reader is referred to the web version of this article.)

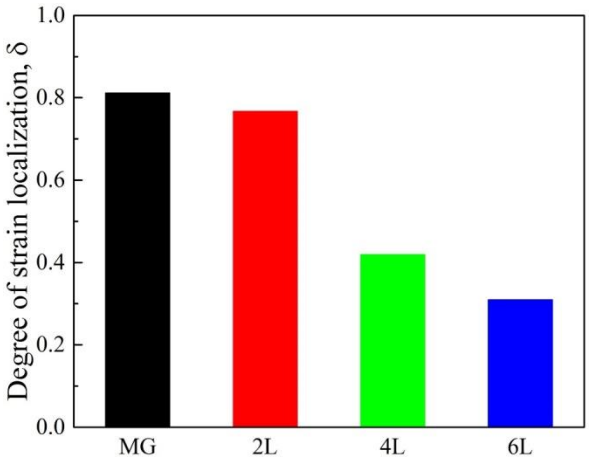

Figure 7. Comparison of the propensity for strain localization for the nanolaminates at an applied strain of 17%.